Droplet Coalescence and Breakage Rates in a Packed Liquid Extraction Column

Coalescence rates for MIBK (methyl isobutyl ketone) droplets in water in a packed column have been measured directly using a novel colorimetric technique. Second-order coalescence and first-order breakage rate constants were derived from the results using a discrete population balance model and were correlated in terms of droplet diameter and dispersed-phase holdup. It is shown that the rate constants can be used to predict the steady-state droplet-size distribution and coalescence rates. They were also used in a theoretical study of mass transfer for a typical polydisperse system, which showed that repeated droplet coalescence and breakage leads to some reduction in column height.

J. A. HAMILTON and H. R. C. PRATT

Department of Chemical Engineering
University of Melbourne
Parkville, Australia

SCOPE

Deviations from ideal plug-flow behavior of liquid extraction columns arise from two causes, *viz.*, axial dispersion of one or both phases, and the polydisperse nature of the dispersed phase. The effect of axial dispersion, primarily backmixing, on performance can be accounted for by the use of either a "diffusion" or a "backflow" model (Sleicher, 1959, 1960; Miyauchi and Vermeulen, 1963). A method for the scale-up of columns using these models has been proposed by Pratt and Garg (1981).

The effect of polydispersity is quite different and arises from the range of droplet sizes present, each with differing specific surfaces, mass transfer coefficients, and velocities. As a result, the smaller droplets approach equilibrium more rapidly than the larger sizes, leading to a reduced performance (Olney, 1964); this has been loosely termed "forward mixing" (Rod, 1966). The extent of this loss in performance would be expected to be lowered by repeated coalescence and breakage of the droplets, due to the tendency to average the droplet solute concentration over the column cross-section. Theoretical computations by Chartres and Korchinsky (1975) confirmed that this was so, although in the absence of measured coalescence rates they expressed these in terms of an assumed "coalescence height."

There is, therefore, a need for actual measured values of coalescence and breakage rates to enable this effect to be investigated in depth. Recently, Hamilton and Pratt (1980) described a novel colorimetric method for the measurement of coalescence rates, involving the formation of red droplets on coalescence of previously size-equilibrated droplet streams containing respectively green and yellow reagents, and preliminary data were reported for a packed column. More extensive data are presented here, and a model is proposed for their interpretation.

CONCLUSIONS AND SIGNIFICANCE

Coalescence data obtained for size-equilibrated methyl isobutyl ketone (MIBK) droplets in water in a column packed with 12.5 mm Raschig rings have been interpreted in terms of second-order coalescence and first-order breakage rate constants using a discrete population balance model. This is based on droplet-size intervals with mean diameters of adjacent sizes in the ratio $2^{1/3}$; in the present case nine intervals were assumed, with diameters of 0.712 to 4.59 mm inclusive. The model equations, in matrix form, were solved for the rate constants, which were correlated as follows in terms of droplet diameter, d_j, and total dispersed phase holdup, x_d:

$$\text{Coalescence: } k_j = 0.0546\, d_j^{-0.36}\, c_d^{-0.50}$$

$$\text{Breakage: } K_j = 1.704\, d_j^{0.24}\, x_d^{0.37}$$

It is shown that the steady-state droplet-size distribution and coalescence rates can both be predicted from the rate constants using a Monte Carlo random selection procedure. This method was extended to simulate the rate of extraction of 5% aqueous acetic acid with MIBK in order to determine the effect of droplet interactions on column performance. The results confirmed that droplet coalescence and breakage reduce the adverse effect of polydispersivity; thus, the predicted packing heights for the 10% holdup case were in the ratios of 1.032: 1.000:0.914 for zero, the measured, and infinite coalescence/breakage rates respectively in the absence of continuous-phase backmixing, neglecting differences in velocities of the various droplet sizes.

INTRODUCTION

Experimental data on interdroplet coalescence rates are sparse and have been confined mostly to agitated vessels at low holdup of dispersed phase. Some work has also been done on the theoretical modelling of droplet coalescence and breakage rates in dispersed systems in terms of continuous population balances, e.g., by Valentas et al. (1966) and Bajpai et al. (1976); work in both areas has been reviewed by Hamilton and Pratt (1980) and Hamilton (1981).

Jiricny et al. (1979a) have recently proposed a discrete population balance model for column contactors, different from the one to be presented here, and described an iterative algorithm for its solution (1979b); in the absence of experimental data, they used assumed values of the model parameters. Sovova and Prochazka (1981) compared the continuous and discrete models as applied to a batch stirred tank, again using assumed parameter values. Sovova (1981) compared published experimental droplet-size data for stirred tanks with Coulaloglou and Tavlarides' theoretical expressions (1977) for the coalescence and breakage rate constants, and proposed a modified formula for the former.

It is clear that a need has existed for some time for a direct method of measurement of interdroplet coalescence rates in extraction columns. This has been provided recently by a method described by Hamilton and Pratt (1980), who also presented pre-

Present address of J. A. Hamilton: C/-Shell Refining Australia Pty. Ltd., Corio, Victoria 3214, Australia.

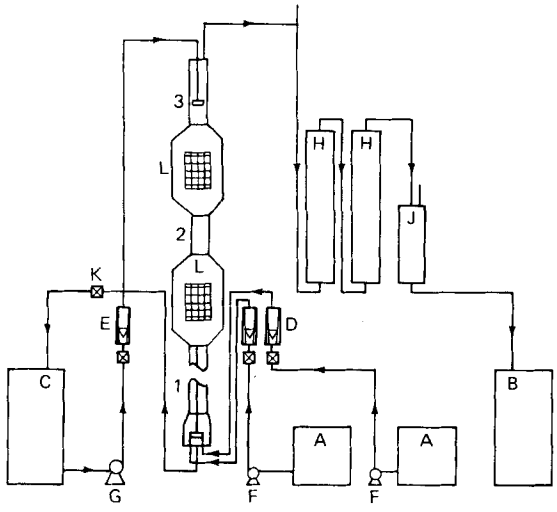

1 Equilibration Section
2 Coalescence Section
3 Interface Section
A Solvent Stock Tanks (80 L)
B Solvent Receiving Tank (160 L)
C Water Stock Tank (160 L)
D Rotameters (0.2-1.5 L/min)
E Rotameter (0.3-3.0 L/min)
F Solvent Pumps (0.25 hp)
G Water Pump (0.11 hp)
H Activated Carbon Columns
J Sand Filter
K Interface Control Valve
L Photographic Window

Figure 1. General arrangement of equipment.

liminary data for the system MIBK–water in a packed column. Their method involved the size equilibration of separate streams of dispersed-phase droplets containing respectively dithizone (green) and nickel di (ethyl xanthate) (yellow) in a section of packed column provided with longitudinal partitions; the droplets were then allowed to mingle and to enter a second column section containing a variable height of packing, when the coalescence of green with yellow droplets gave red droplets, whose proportion was determined photographically. Additional data for the same system are given below and are interpreted theoretically in terms of coalescence and breakage rate constants using a novel form of population balance model.

EXPERIMENTAL

Equipment

The column, Figure 1, comprised a 1.0 m long size equilibration section of 72.45 mm precision bore QVF glass tube divided longitudinally into quadrants by means of 20 swg SS partitions; the coalescence and interface sections were 0.3 and 0.5 m lengths respectively of 75 mm nominal bore tube. Both equilibration and coalescence sections were packed with 12.5 × 2 mm Raschig rings, the height in the latter being varied from 5 to 30 cm. The photographic windows had parallel sections 165 mm wide × 25 mm deep and were fitted with 130 × 160 mm glass windows provided with millimeter scales.

The solvent distributor was divided into quadrants, whose opposite pairs were fed with separate solvent flows. The general arrangement of the equipment is shown in Figure 1; further details are given by Hamilton and Pratt (1980).

Materials

Commercial grade MIBK was used as dispersed phase and deionized water as continuous phase; both were presaturated by circulation through the column before use. The spent solvent was passed through beds of ICI "Darco" grade of activated carbon before reuse. Measurements of interfacial tension between the phases using a du Noüy balance gave values close to 13 dyne/cm, with variations well within the instrument's limit of error, both without and with reagents present and before and after passage through the activated carbon bed.

The diphenylthiocarbazone ("Dithizone") was obtained from laboratory suppliers and the nickel di (ethyl xanthate) was prepared by precipitation and recrystallization from ethanol. The reagent concentrations used were 0.1 and 0.05 g/L respectively, i.e., in a stoichiometric ratio of approximately 1:3.5. The dithizone was added to the solvent immediately before a run, in view of its instability.

Procedure

After stabilising conditions in the column, two photographs were taken of the lower window and 4–5 of the upper window on Kodak Ektachrome 35 mm ASA 160 Professional Color Slide film using a camera with a 50 mm F 1.8 lens and $1/250$ s exposure. Illumination was provided by means of 500 W Photoflood lights reflecting from opaque white screens behind the windows.

The color slides were projected on to a screen using a suitable magnification as determined by the scales on the windows. All droplets within grid areas selected at random, numbering at least 150 per slide, were counted and their color and size of minor and major axes recorded; their effective diameters were then calculated as $\sqrt[3]{d_1^2 d_2}$. Taking the smallest size as 0.712 mm, they were classified into nine size ranges with mean diameters based on intervals of $2^{1/3}$, i.e., so that the mean droplet volume of any size is twice that of the size below. The results were used to calculate the Sauter mean diameters, d_{32}, and the frequency distributions of both red and of all droplets.

RESULTS

Three series of runs were carried out using an aqueous flow rate of 9.65 cm^3/s, and dispersed-phase flows of 3.34, 7.34 and 10.97 cm^3/s; the corresponding estimated values of the dispersed-phase holdup were 4.8, 10.6 and 17.0% respectively (cf., Gayler *et al.*, 1953). In each series of runs four or five packing heights, from 5.0 to 30.0 cm inclusive, were used. Coalescence in the lower window was negligible throughout.

It was found that the data could be better fitted with the actual packing height reduced by 2.5 cm, suggesting that the first two courses of packing were ineffective in promoting coalescence. In view of scatter, the data for each droplet size were smoothed by fitting to the following equation by means of l_1 norm regression analysis (Barrodale and Roberts, 1974)

$$1 - f_j = \frac{1}{(1 + Ah')^n} \tag{1}$$

where $h' = (h - 2.5)$. The resulting values of the constants n and A were used to calculated smoothed curves of f_j vs. h'. Values of the coordinates of these curves, which are based on more extensive data than those given earlier by Hamilton and Pratt (1980), are summarized in Table 1. Typical plots, comparing the experimental data with the smoothed curves, are shown in Figure 2 for the 10.6% holdup case.

INTERPRETATION OF RESULTS

Basis of Model

The model was based on two sets of population balances over each of a set of size intervals, one involving the droplet-size distribution and the other the rate of formation of red droplets. The assumptions involved were as follows:

(1) The droplet-size distribution can be expressed as a series of discrete-size intervals such that the mean diameters of adjacent sizes are in a ratio of $2^{1/3}$.

(2) Only coalescence between droplets in the same, and in adjacent-size intervals are considered.

(3) The coalescence rate for two droplets of size j can be expressed in terms of a second-order rate constant k_j, with droplet number concentration as a driving force. The resulting droplets will all be of size $j + 1$.

(4) The rate constant, k_j^{j-1}, for the coalescence of a droplet of size j with one of size $j - 1$ is given by

$$k_j^{j-1} = 0.50(k_j + k_{j-1}) \tag{2}$$

(5) Of coalescences of droplets of size j with $j - 1$, one half result

TABLE 1. SMOOTHED VALUES OF FRACTION OF RED DROPLETS AS FUNCTION OF HEIGHT $h'(=(h-2.5))$

j	Diam. mm	Fraction Red Droplets at Height h'(cm) of: 5.0	10.0	15.0	20.0	30.0
		(i) Series 1: 4.8% Holdup				
1	0.712	0.211	0.371	0.495	0.590	0.725
2	0.897	0.315	0.519	0.655	0.748	0.859
3	1.130	0.256	0.438	0.569	0.666	0.793
4	1.424	0.274	0.464	0.598	0.694	0.816
5	1.794	0.302	0.502	0.638	0.732	0.847
6	2.260	0.440	0.669	0.795	0.868	0.940
7	2.847	0.401	0.625	0.757	0.837	0.921
8	3.587	0.526	0.755	0.864	0.920	0.969
9	4.520	0.936	0.990	0.997	0.999	1.00
		(ii) Series 2: 10.6% Holdup				
1	0.712	0.528	0.756	0.865	0.921	0.969
2	0.897	0.471	0.702	0.822	0.889	0.952
3	1.130	0.470	0.674	0.781	0.843	0.908
4	1.424	0.458	0.686	0.808	0.878	0.945
5	1.794	0.505	0.671	0.754	0.803	0.860
6	2.260	0.522	0.625	0.751	0.828	0.910
7	2.847	0.575	0.798	0.895	0.942	0.979
8	3.587	0.732	0.884	0.957	0.961	0.981
9	4.520	0.933	0.956	0.965	0.971	0.977
		(iii) Series 3: 17.0% Holdup				
1	0.712	0.553	0.753	0.846	0.896	0.944
2	0.897	0.454	0.681	0.803	0.872	0.941
3	1.130	0.573	0.744	0.822	0.866	0.913
4	1.424	0.531	0.708	0.794	0.843	0.897
5	1.794	0.486	0.716	0.834	0.898	0.957
6	2.260	0.560	0.785	0.886	0.936	0.976
7	2.847	0.720	0.900	0.948	0.980	0.994
8	3.587	0.765	0.909	0.955	0.974	0.989
9	4.520	0.946	0.981	0.990	0.994	0.997

in a droplet of size $j+1$ and the other half remain in size j.

(6) The breakage rate of droplets of size j, giving pairs of droplets of size $j-1$, can be expressed by means of a first-order rate constant K_j.

Droplet Number Balance

The balance over a size interval j comprises four terms, as follows:

(a) The number of droplets entering size j from below due to coalescences of: (i) two droplets of size $j-1$; and (ii) droplets of size $j-1$ with $j-2$, one-half of which give size j.

(b) The number leaving size j by coalescence, due to coalescences of: (i) two droplets of size j; (ii) droplets of size j with $j+1$; and (iii) droplets of size j with $j-1$, one-half of which form size $j+1$.

(c) The number entering size j from $j+1$ by breakage.

(d) The number leaving size j by breakage to size $j-1$.

The rate of change of number concentration, dn_j/dt, is related to column height by noting that

$$dh/dt = \bar{v}_r \tag{3}$$

where $\bar{v}_r$, the mean droplet velocity relative to stationary coordinates, is given by

$$\bar{v}_r = U_d/\epsilon x_d \tag{4}$$

It will be assumed that all droplets have the same average velocity, $\bar{v}_r$; the justification for this will be discussed later. From Eqs. 3 and 4 therefore

$$\frac{dn_j}{dt} = \frac{U_d}{\epsilon x_d}\frac{dn_j}{dh} \tag{5}$$

On collecting terms, the droplet population balances become

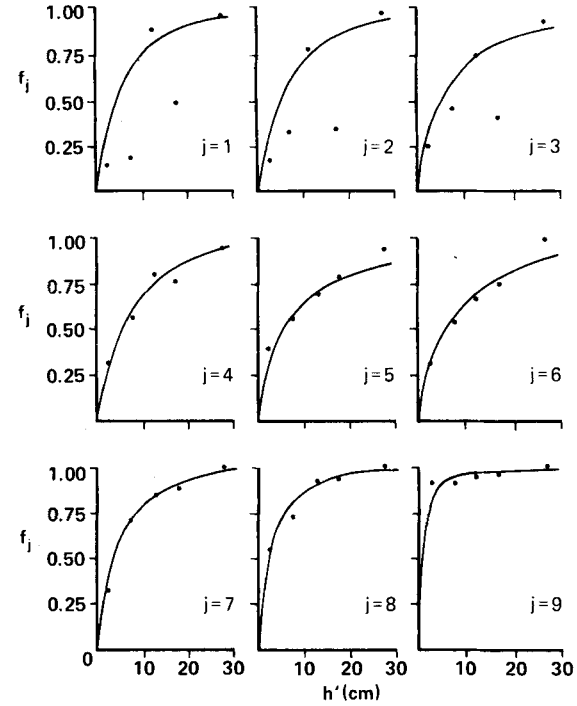

Figure 2. Fraction of red droplets vs. packing height for 10.6% holdup: comparison of experimental data with smoothed curves [$h' = (h - 2.5)$ cm].

$$\frac{U_d}{\epsilon x_d}\frac{dn_j}{dh} = \Delta_j = C_{j,j-2}k_{j-2} + C_{j,j-1}k_{j-1} + C_{j,j}k_j + C_{j,j+1}k_{j+1} + B_{j,j}K_j + B_{j,j+1}K_{j+1} \tag{6}$$

where

$$C_{j,j-2} = 0.25n_{j-2}n_{j-1}$$

$$C_{j,j-1} = n_{j-1}(n_{j-1} + 0.25n_{j-2} - 0.25n_j)$$

$$C_{j,j} = -n_j[2n_j + 0.5(0.5n_{j-1} + n_{j+1})]$$

$$C_{j,j+1} = -0.5n_{j+1}n_j$$

$$B_{j,j} = -n_j$$

$$B_{j,j+1} = 2n_{j+1}$$

Red Droplet Balance

A balance is similarly made of the number of red droplets present as a function of height of packing. Using the symbols G_j, Y_j and R_j to designate green, yellow and red droplets of size j, this comprises the following terms:

(a) The gain in R_j due to coalescences of: (i) Y_{j-1} with G_{j-1}; (ii) Y_{j-1} with G_{j-2} or *vice versa*, one-half giving R_j; (iii) R_{j-1} with any color of size $(j-1)$; (iv) R_{j-1} with any color of size $(j-2)$, one-half giving R_j; (v) any droplets of sizes j and $j-1$ which stay in size j but change color; and (vi) R_{j-2} with Y_{j-1} or G_{j-1}, one-half giving R_j.

(b) The loss in R_j by: (i) twice the number of coalescences of R_j with R_j; coalescences of (ii) R_j with Y_j or G_j; (iii) R_j with any color of size $j-1$, one-half of which form size $j+1$; and (iv) R_j with any color of size $j+1$.

(c) The gain in R_j due to breakage of R_{j+1} droplets.

(d) The loss in R_j due to breakage of R_j droplets.

The terms in (a) (iv) and (vi) arise because the reagent concentrations used result in a measurable colour change for coalescences between droplets in adjacent sizes.

The red population balance thus becomes

TABLE 2. VALUES OF RATE CONSTANTS

j	d_j (mm) x_d=	Coalescence Constant, k_j ($cm^3 \cdot s^{-1}$)* 0.048	0.106	0.170	Breakage Constant, K_j (s^{-1})* 0.048	0.106	0.170
1	0.712	1.123	0.797	(0.0)	0.158	0.312	0.885
2	0.897	0.072	0.739	0.250	0.534	0.526	0.283
3	1.130	0.583	(0.0)	0.542	0.224	0.702	0.632
4	1.424	(0.0)	0.749	(0.0)	0.332	0.253	1.013
5	1.794	0.434	0.336	0.229	(0.124)	0.683	(0.196)
6	2.260	0.421	(0.0)	0.041	0.496	0.419	0.542
7	2.847	(0.0)	0.242	0.216	0.531	(0.107)	0.254
8	3.587	0.475	0.058	(0.0012)	0.180	0.550	1.067
9	4.520	0.503	0.858	(0.588)	1.118	0.661	0.581

* Bracketed values were omitted in the final correlations.

$$\frac{U_d n_j}{\epsilon x_d}\frac{df_j}{dh} = \Delta_j^R = C_{j,j-2}^R k_{j-2} + C_{j,j-1}^R k_{j-1} + C_{j,j}^R k_j + C_{j,j+1} k_{j+1} + B_{j,j}^R K_j + B_{j,j+1}^R K_{j+1} \quad (7)$$

where

$$C_{j,j-2}^R = n_{j-1} n_{j-2}(0.125F_{j-1}F_{j-2} + 0.25f_{j-1} + 0.25f_{j-2}F_{j-1})$$

$$C_{j,j-1}^R = n_{j-1}[F_{j-1}(0.5n_{j-1}F_{j-1} + 0.125n_{j-2}F_{j-2} + 0.125n_jF_j + 0.25n_{j-2}f_{j-2}) + n_{j-1}f_{j-1} + 0.25f_{j-1}(n_{j-2} + n_jF_j) - 0.25n_jf_j]$$

$$C_{j,j}^R = n_j[n_{j-1}F_j(0.125F_{j-1} + 0.25f_{j-1}) - f_j(2n_jf_j + n_jF_j + 0.25n_{j-1} + 0.5n_{j+1})]$$

$$C_{j,j+1}^R = -0.5n_jf_jn_{j+1}$$

$$B_{j,j}^R = -n_jf_j$$

$$B_{j,j+1}^R = 2n_{j+1}f_{j+1}$$

The values of n_j in Eqs. 6 and 7 are obtainable from the experimental data using the following expression relating the total droplet volume to the dispersed-phase holdup

$$x_d = \sum_{i=1}^{M} n_i \pi d_i^3/6 \quad (8)$$

Thus, solving for n_j, noting that $n_j \equiv n_i$, gives

$$n_j = \frac{6x_d}{\pi \sum_{i=1}^{M} n_i d_i^3/n_j} \qquad j = 1, 2, \ldots M \quad (9)$$

Hence the values of n_j were calculated for each droplet size from the ratios n_i/n_j obtained from the experimental data, using the values of x_d given under "Results."

Matrix Formulation

Equations 6 and 7 can be combined and expressed in matrix form as follows

$$Ax = z \quad (10)$$

where A is a $2M \times 2M$ partitioned matrix, x a vector of the k_j and K_j values and z a vector of the Δ_j and Δ_j^R values. Equation 11 shows this in fully expanded form for $\Delta = 0$, i.e., for a steady-state size distribution; A is seen to comprise two quadridiagonal submatrices of coalescence terms and two bidiagonal ones of breakage terms.

The true coalescence rates correspond to the gradients of the plots of f_j vs. h' in Figure 2 at $h' = 0$, where only green and yellow droplets are present. However, the red droplet balances are meaningless for zero height since then $f_j = 0$ for all sizes. Values of Δ_j^R were, therefore, obtained from the gradients at $h' = 2.5$ cm, i.e., $h = 5.0$ cm, the smallest height used in the experiments; these were determined by differentiation of Eq. 1 using the appropriate values of A and n.

Before solving Eq. 8 it is necessary to ensure that no droplets are lost to the system by further breakage of the smallest or coalescence of the largest sizes considered. Equations 6 and 7 were therefore written for the size below $j = 1$, designated size $j = 0$, setting $K_o = 0$, and similarly for size $j = 10$, setting $k_{10} = 0$; this inferred that $n_j = 0$ for $j < 0$ or > 10. The equations for $j = 0$ were solved for k_o, which was substituted into those for $j = 1$ and 2 to eliminate k_o. In the same way, K_{10} was eliminated from the equations for $j = 9$ using those for $j = 10$.

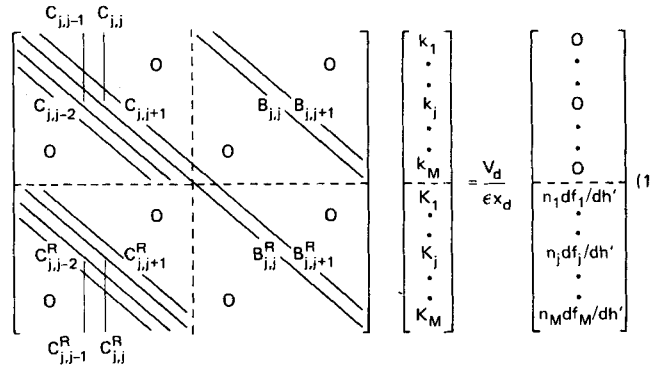

(11)

Solution of Model Equations

It was not possible to solve Eq. 10 directly for the rate constants since matrix A was found to be singular. [Garg (1982) later found the reason for this; see also Garg and Pratt (1983).] However, the solution can alternatively be expressed as an optimization problem by introducing an error vector, ϵ, into this equation as follows

$$\epsilon = Ax - z \quad (12)$$

The required solution is then the value of x which minimises the sum of squares of ϵ (i.e., the l_2-norm), as follows

$$\phi_2 = \epsilon^T\epsilon = (Ax - z)^T(Ax - z) = x^TA^TAx - 2z^TAx + z^Tz \quad (13)$$

The objective function ϕ_2 is therefore quadratic in x so that the latter can be obtained by quadratic programming. Equation 13 was solved using a multipurpose optimization program (MPOS), available as a library program, giving the results summarized in Table 2. The only constraint introduced in obtaining these results was that the rate constants must be nonnegative. The zero values which appear in Table 2, arose because the optimization program left a zero value when no improvement could be effected by a discrete increase in value of the rate constant.

Correlation of Rate Constants

Table 2 indicates an apparent oscillatory tendency of the rate constants, the reasons for which will be discussed later. However, it is clear that both are functions of droplet size and holdup, and

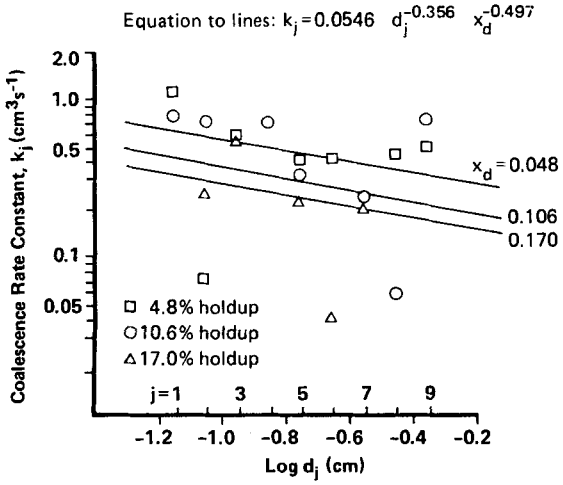

Figure 3. Correlation of derived droplet coalescence rate constants.

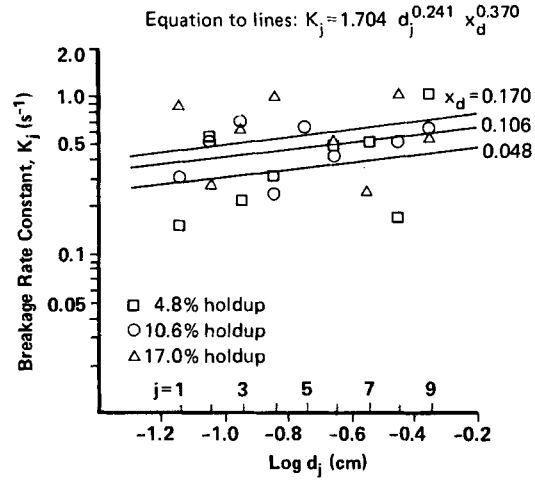

Figure 4. Correlation of derived droplet breakage rate constants.

they were therefore fitted to power functions of these variables by regression analysis. In fitting the coalescence rate constants, the zero values were first omitted; the data were then refitted after omitting the two additional bracketed values in Table 2, lying outside the 90% confidence limits. The final result was then

$$k_j = 0.0546 d_j^{-0.36} x_d^{-0.50} \tag{14}$$

where d_j is in cm and x_d is expressed as fractional holdup.

The breakage rate constants showed somewhat greater scatter than the coalescence constants, presumably because they were not obtained by direct measurement. The values were correlated in the same way, omitting three values outside the 85% confidence limits; this narrower limit was selected in order to improve the sensitivity of the fit. The resulting expression was

$$K_j = 1.704 d_j^{0.24} x_d^{0.37} \tag{15}$$

Equations 14 and 15 are plotted in Figures 3 and 4, which also show the original data points.

APPLICATIONS OF RATE CONSTANTS

A knowledge of the rate constants is of particular value in studies of the effect of droplet coalescence and breakage on mass transfer in extractors. However, before attempting such a study it is of interest to investigate their applicability to the prediction of the steady-state droplet-size distribution and coalescence rates. For this purpose, it is possible to solve the systems of equations represented by Eqs. 6 and 7 numerically for the n_j and f_j, as shown by Garg and Pratt (1983). However, it was decided in the present instance to employ a Monte Carlo random selection procedure, since an extension of this method was to be used later in the mass transfer study.

Steady-State Size-Distribution and Coalescence Rate

The total number of droplet interactions, i.e., coalescences of equal and of adjacent sizes, and of breakages, in height Δz per unit void volume of packing is given by

$$\Sigma_T = \frac{\Delta z}{\bar{v}_r}\left[\sum_{j=0}^{M} k_j n_j^2 + \sum_{j=1}^{M} k_j^{j-1} n_j n_{j-1} + \sum_{j=1}^{M+1} K_j n_j\right] = \left[\sum_{j=0}^{M} C_j + \sum_{j=1}^{M} C_j^{j-1} + \sum_{j=1}^{M+1} B_j\right] \tag{16}$$

The relative numbers of each type of interaction are given by the ratios of the individual terms on the righthand side of Eqn. 16 to Σ_T, and random numbers were therefore allocated in these proportions to establish the probabilities of coalescences of either type, or breakage. Having thus selected a particular type of interaction, the droplet size range involved was assessed from further random numbers allocated amongst the possible values of C_j, C_j^{j-1} or B_j. Finally, when considering the rate of red droplet formation, the probability of each droplet being yellow, green or red was also assessed.

The program as written involved 11 droplet size intervals; i.e., including $j = 0$ and 10 to minimize end effects. Thus, 44 storage locations were required, with four for each size to contain the numbers of green, yellow, red and total droplets respectively. The numbers of droplets in the appropriate locations were adjusted after each interaction; thus, on coalescence of a yellow droplet of size $j = 5$ with a green one of size $j = 4$, these two locations would be debited with one droplet each, and the resulting red droplet credited to size $j = 5$ or 6 on a 50% probability basis. The random selection process was assumed to operate over incremental column heights of 0.10 cm after which the size distribution and probabilities were recalculated to minimize cumulative errors. The steps involved in the computation are summarized in Appendix A.

The input data to the program were the experimental size distributions for the 11 size intervals, for each of the three values of the holdup used. In order to compare the simulated with the experimental values of the fraction of red droplets present, the former were fitted to Eq. 1 for heights up to 5.0 cm. This height restriction was adopted since in the simulation a "red" droplet, once formed, would stay red despite the number of further simulated coalescences it underwent with yellow and green droplets, whereas experimentally it was not possible to recognize the red color after more than two or three such further coalescences.

The calculations were repeated using the rate constant values given in Table 2 instead of the smoothed values obtained from Eqs. 14 and 15, but the differences in the results were small. A comparison of the experimental and predicted results is shown in Figure 5 for the 10% holdup case; the full results are given by Hamilton (1981). A comparison of the experimental values of the Sauter mean diameter with those predicted by computer simulation is given in Table 3.

Effect on Mass Transfer

Theoretical studies of the effect of polydispersity on mass transfer were conducted for the extraction of 5.0% w/v aqueous acetic acid with MIBK in a column packed with 12.5 mm Raschig rings to give a raffinate containing 0.1 or 1.0% acetic acid. Equilibrium data for this system, given by Vermijs and Kramers (1954), were fitted to a straight line relationship by least squares regression as follows

$$c_y^* = 0.545 c_x \tag{17}$$

Values of the holdup of 5.0, 10.0 and 17.0% were assumed, together with an extraction factor, $E = U_c/mU_d$, of 0.70; the latter corresponds to a phase flow ratio, U_c/U_d, of 0.3815.

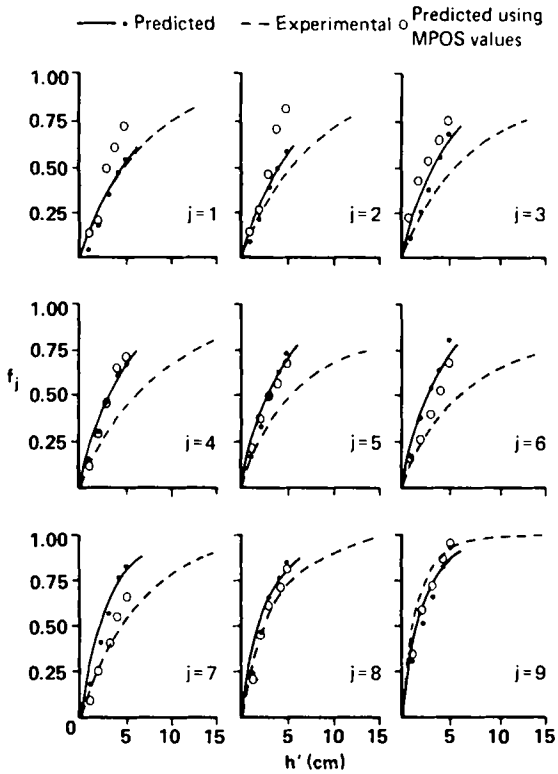

Figure 5. Comparison of experimental and calculated fraction red curves (10.6% holdup).

TABLE 3. COMPARISON OF PREDICTED AND EXPERIMENTAL VALUES OF d_{32} (mm)

Holdup %	d_{32} (Experimental) Inlet*	Exit+	d_{32}, Computed Using Rate Constants from Eqs. 14-15	Table 2
4.8	2.68	3.18	3.46	3.51
10.6	3.18	3.52	3.46	3.41
17.0	3.20	3.42	3.53	3.32

* Lower window.
\+ Upper window.

The mass transfer simulation was undertaken by a stepwise procedure using increments of column height of 0.10 cm starting from the solvent inlet, at which the measured steady-state droplet-size distribution was assumed. Blocks of storage locations were allocated to each size in proportion to the number of droplets in that size, each location storing the solute concentration in a single droplet. In all, 1,500–2,000 storage locations were used, including about 10% spares. Plug flow of the dispersed phase was assumed, i.e., with all droplets moving at a rate given by Eq. 4. Both plug flow and backmixing of the continuous phase were considered; in the latter case, the Peclet numbers were obtained from the correlation of Pratt and Anderson (1977).

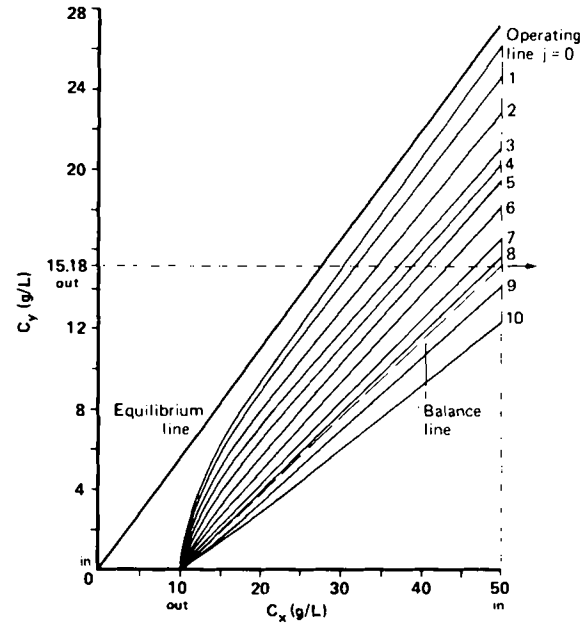

Figure 6. Predicted operating lines for each droplet size range in the extraction of aqueous acetic acid from 5.0% w/v to 1.0%, with allowance for droplet coalescence and breakage (plug flow, 10% holdup).

The procedure involved first the calculation of the change in concentration of *each* droplet over the height interval Δh, followed by the mean dispersed and continuous phase compositions, using an iterative procedure. Coalescence and breakage events were then selected in the appropriate proportions for the height increment using random numbers, followed by the sizes and concentrations of the droplets undergoing interactions; the latter were replaced in the storage locations by negative flags, and the concentration of the droplets resulting from coalescence or breakage were inserted into vacancies in the appropriate stores. Details of the program are given in Appendix B, together with the mass transfer coefficients used. Four different cases were considered as follows:

(i) Polydispersion with no droplet coalescence or breakage.

(ii) Polydispersion with the measured coalescence and breakage rates.

(iii) Polydispersion with "infinite" coalescence and breakage rates.

(iv) Monodispersion with droplet size equal to the Sauter mean diameter, d_{32}, of the polydispersion.

The first case corresponds to a constant size distribution with no droplet interactions, and the third to lateral equalisation of the droplet concentrations at every cross-section.

The results of the computation for the 10% holdup case with 0.1% acetic acid in the raffinate are summarized in Table 4. This shows that the packing heights are in the ratios 1.032:1.00:0.914 for cases (i)–(iii) respectively in the absence of continuous-phase backmixing. The corresponding concentration profiles for the various droplet-size fractions with 1.0% acetic acid in the raffinate are shown in Figure 6 for case (ii).

TABLE 4. EFFECT OF DROPLET COALESCENCE AND BREAKAGE ON COLUMN HEIGHT (10% HOLDUP CASE)

Case No.	Simulation	Without Backmixing N_{od}	H.T.U. cm	h cm	Δh* %	With Backmixing+ N_{od}	H.T.U. cm	h cm	Δh* %
(i)	No coalescence	6.426	39.04	250.9	12.9	10.32	39.72	409.9	9.2
(ii)	Measured coalescence & breakage rates	6.428	37.82	243.1	9.4	10.43	39.10	407.8	8.7
(iii)	Infinite coalescence	6.427	34.59	222.3	0	10.85	34.58	375.2	0
(iv)	Monosized Dispersion	6.426	35.51	228.2	2.6	10.74	35.52	381.5	1.7

* $\Delta h(\%) = 100(h - h_\infty)/h_\infty$, where h_∞ corresponds to case (iii).
\+ $E_c = 1.47\ \text{cm}^2\text{-s}^{-1}$.

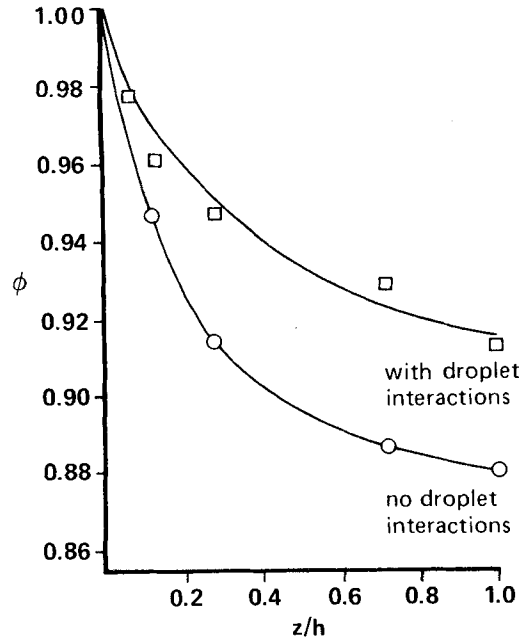

Figure 7. Relative mass transfer rate, Φ, vs. dimensionless height of packing, Z, for the extraction of acetic acid (Figure 6), showing the effect of droplet coalescence and breakage.

DISCUSSION

The experimental method used for measuring coalescence worked very well and gave no indication of any error of principle. Thus, the color change appeared to be immediate, and there was no evidence whatsoever of either reagent transferring via the aqueous phase into droplets containing the other phase, so that their partition coefficients into solvent must be extremely high. Interfacial tension gradient (Marangoni) effects must also have been absent, since careful measurements of interfacial tension between the phases showed no significant differences due to the presence of either reagent or of reaction product.

Statistical variations, on the other hand, were of considerable relevance, and were the cause of the scatter of the fraction red data in Figure 2. These comprised primarily "sampling" errors, and effects due to the randomness of the packing. The former, which resulted from irregularities in the passage of the droplet swarms through the windows, were minimized by averaging the data obtained from several photographs. The latter, the result of fluctuations in orientation of the packing elements and in voidage, lead to appreciable variations in performance on repacking, as is well known. The object of the preliminary smoothing of the data was to compensate for these effects.

The effect of multiple coalescences, that is, of red with further green or yellow droplets, was also taken into account, both by the use of an appreciable stoichiometric excess of the nickel reagent to minimize masking of the red color by the more intense green of the dithizone, and by determining the gradients, df_j/dh', at the smallest practicable value of h'. Evidence of the occurrence of multiple coalescences is provided by the increasing deviation of the predicted fraction red curves in Figure 5, above the experimental values, with increase in height.

The oscillations in the values of the rate constants in Table 2 almost certainly resulted from the truncation of the droplet-size distribution at the two ends of the size range. Although this led to considerable scatter of the data points in Figures 3 and 4, it is of interest that the differences in the predicted values of f_j using the smoothed and the direct MPOS values of the rate constants is small, especially at small packing heights, Figure 5. The same is true of the predicted and measured values of the Sauter mean diameter, d_{32}, in Table 3 for the two higher values of the holdup. The experimental values for the 6.3% holdup case are somewhat lower than predicted, however, suggesting as suspected that size equilibration was not quite complete in this case.

The correlations of the rate constants in Eqs. 14 and 15 are partial, in the sense that they do not include physical properties. Of these, the density difference and interfacial tension are likely to be the most important. On this basis, noting that the flow rates of the phases are taken into account by incorporating the holdup, dimensional analysis indicates that the data should be correlated by expressions of the following types

$$\frac{k_j^4 \Delta\rho^5 g^3}{\gamma^5} = C_1 \left(\frac{d_j^2 \Delta\rho g}{\gamma}\right)^m x_d^n \tag{18}$$

and

$$\frac{K_j^4 \gamma}{\Delta\rho g^3} = C_2 \left(\frac{d_j^2 \Delta\rho g}{\gamma}\right)^p x_d^q \tag{19}$$

Values of the exponents in these equations are obtainable from those in Eq. 14 and 15. It is probable that the phase viscosities and the continuous-phase density would have small influences also, requiring additional dimensionless groups. In an attempt to determine the effect of $\Delta\rho$ and γ, preliminary tests of the present color reaction using odorless kerosene, toluene, carbon tetrachloride and butyl acetate as solvent were carried out, but it was found that the reaction time was too slow to be of use, although the addition of 10–20% of MIBK to the kerosene effected some improvement. This slow reaction may be due to the low solubility of one or both reagents, coupled with low polarity of the solvents.

Although the computer predictions of packing height for acetic acid extraction are unlikely to be accurate in absolute terms due to uncertainties in the droplet mass transfer rates (Korchinsky and Cruz-Pinto, 1979), the results are of comparative value in indicating the likely effects of polydispersivity and droplet coalescence on performance. The concentration profiles for individual droplet fractions shown in Figure 6 are of the same form as those predicted by Rod (1966) who, however, also included the effect of differing droplet velocities. Such differences would undoubtedly increase the effect of droplet coalescence and breakage on performance. However, it can be shown from the present results that the mean droplet lifetime between such interactions is only 0.67 s for the 10% holdup case; since the droplets are frequently brought to rest by collision, differences in velocity may well be very small. Support for this view is provided by the analogous case of the hindered settling of solid suspensions, in which all particles deposit at the same rate irrespective of size.

Rod (1966) considered that the loss in performance due to "forward mixing," i.e., polydispersivity, arises from a reduction in effective driving force, and he gave a plot of the ratio of the driving force relative to the plug flow value against dimensionless height. However, it can be shown that the correctly weighted overall driving force in Figure 6 is identical with the plug flow value, and that in reality the performance loss arises from the differing specific surfaces and mass transfer coefficients of the various droplet-size fractions. On this basis the ratio Φ, the mass transfer rate relative to that for infinite rates of coalescence and breakage, is given by

$$\Phi = \frac{\sum_j (N_j \pi d_j^3/6) K_{od,j} a_j (c_y^* - c_{y,j})}{\sum_j (N_j \pi d_j^3/6) K_{od,j} a_j (c_y^* - c_y)_p} \tag{20}$$

where $(c_y^* - c_y)_p$ is the driving force corresponding to the plug flow operating line. Plots of Φ vs. dimensionless height, obtained from the present results for 10% holdup, are shown in Figure 7. The scatter of the points in the upper plot results from the use of the random selection process in allowing for droplet coalescence and breakage.

The very short droplet lifetime of 0.67 s referred to above indicates that the interaction rate is very large; thus, for a droplet population of 3,000 and 10% holdup corresponding to a column of 29 cm diameter, there are 1,590 interactions per cm of travel, of which 50% are coalescences. It is, therefore, somewhat surprising that the predicted effect of these on packed height is only 3.2%,

as compared with 11.4% for "infinite" coalescence. However, appreciable error may be involved in the use of mass transfer coefficients for isolated freely-rising droplets, and there is an urgent need for data relating to the droplet "swarms" present in real extraction columns.

NOTATION

A = constant in Eq. 1
$\mathbf{A}$ = matrix defined by Eq. 11
a_j = $6/d_j$, specific surface of droplet of size j, cm^{-1}
B_j = number of breakages of droplets of size j per unit void volume of packing (Eq. 16), cm^{-3}
C_1, C_2 = constants in Eqs. 18 and 19
C_j = number of coalescences of droplets of size j per unit void volume of packing (Eq. 16), cm^{-3}
C^j_{j-1} = number of coalescences of droplets of size j with size j-1 per unit void volume of packing (Eq. 16), cm^{-3}
c_x, c_y = solute concentrations in aqueous and solvent phases respectively, $g \cdot L^{-1}$
d = droplet diameter, cm
d_j = mean diameter of jth droplet size range, cm
d_1, d_2 = major and minor axes of ellipsoidal droplet, cm
d_{32} = Sauter (i.e., volume-surface) mean diameter of droplets, cm
E = longitudinal dispersion coefficient, $cm^2 \cdot s^{-1}$
F_j = $(1 - f_j)$
f_j = number fraction of red droplets in size range j
h = height of packing, cm
h_∞ = height of packing for infinite coalescence/breakage rate case, cm
h' = $(h - 2.5)$, cm
K_c, K_d = mass transfer coefficient for continuous and dispersed phase respectively, $cm \cdot s^{-1}$
K_{od} = overall mass transfer coefficient based on dispersed phase, $cm \cdot s^{-1}$
K_j = first-order rate constant for breakage of droplets of size j, (number of breakages) $s^{-1} \cdot cm^{-3}$ (number of droplets/cm^3)$^{-1}$ = s^{-1}
k_j = second-order rate constant for coalescence of two droplets of size j, (number of coalescences) $s^{-1} \cdot cm^{-3}$ (number of droplets/cm^3)$^{-2}$ = $cm^3 \cdot s^{-1}$
k_j^{j-1} = second-order rate constant for coalescence of droplet of size j with one of size $j - 1$, $cm^3 \cdot s^{-1}$
N_{od} = number of plug flow transfer units based on dispersed phase
N_j = total number of droplets in size range j
n = exponent in Eq. 1
n_j = number concentration of droplets of size j, cm^{-3} cm^{-3}
t = time, s^{-1}
U_c, U_d = superficial velocity of phase, $cm \cdot s^{-1}$
$\bar{v}_r$ = droplet velocity relative to stationary coordinates, $cm \cdot s^{-1}$
x = column vector of k_j and K_j values (Eq. 10)
x_d = total fractional holdup of dispersed phase
z = height within packing, cm
$\mathbf{z}$ = column vector of Δ_j and Δ_j^R values (Eq. 10)
Z = z/h, fractional height within packing

Greek Letters

Δ_j, Δ_j^R = see Eqs. 6 and 7
ϵ = fractional voidage of packing
$\boldsymbol{\epsilon}$ = error vector (Eq. 12)
Φ = relative mass transfer rate
Σ_T = total number of droplet interactions per unit void volume of packing, cm^{-3}

Subscripts

c = continuous phase
d = dispersed phase
i = interval number
j = droplet-size range
M = largest droplet-size range considered
m = mean value over height interval
o = continuous phase inlet end, within column
1,2,3. . . = number of size interval

Superscripts

o = continuous-phase inlet end, external to column
$-$ = mean value over all droplets

LITERATURE CITED

Bajpai, R. K., D. Ramkrisha, and A. Prokop, "A Coalescence Redispersion Model for Drop Size Distributions in An Agitated Vessel," *Chem. Eng. Sci.*, **31**, p. 913 (1976).

Barrodale, I., and F. D. K. Roberts, "Solution of an Overdetermined System of Equations in the *l*1 Norm," *Comm. of The ACM*, **17**, p. 319 (1974).

Chartres, R. H., and W. J. Korchinsky, "Modelling of Liquid-Liquid Extraction Columns: Predicting the Influence of Drop Size Distribution," *Trans. Inst. Chem. Eng.*, **53**, p. 247 (1975).

Coulaloglou, C. A., and L. L. Tavlarides, "Description of Interaction Processes in Agitated Liquid-Liquid Dispersions," *Chem. Eng. Sci.*, **32**, p. 1289 (1977).

Garg, M. O., "Measurement and Modelling of Droplet Coalescence and Breakage in a Pulsed Perforated Plate Liquid Extraction Column," Ph.D. Thesis, University of Melbourne, (1982).

Garg, M. O., and H. R. C. Pratt, "Measurement and Modelling of Droplet Coalescence and Breakage in a Pulsed Plate Extraction Column," *AIChE J.*, p. 432 (1984).

Gayler, R., N. W. Roberts, and H. R. C. Pratt, "Liquid-Liquid Extraction: Part IV. A Further Study of Holdup in Packed Columns," *Trans. Inst. Chem. Eng.*, **31**, p. 57 (1953).

Griffith, R. M., "Mass Transfer from Drops and Bubbles," *Chem. Eng. Sci.*, **12**, p. 198 (1960).

Hamilton, J. A., "Droplet Coalescence and Breakage in a Packed Liquid Extraction Column," Ph.D. Thesis, University of Melbourne (1981).

Hamilton, J. A., and H. R. C. Pratt, "Measurement of Droplet Coalescence Rates in a Packed Column Using a Novel Colorimetric Technique," *Proc. Int. Solv. Extn. Conf.*, Paper No. 80-19 (1980).

Jiricny, V., M. Kratky, and J. Prochazka, "Countercurrent Flow of Dispersed and Continuous Phase. I: Discrete Polydispersed Model," *Chem. Eng. Sci.*, **34**, p. 1141 (1979a).

Jiricny, V., M. Kratky, and J. Prochazka, "Countercurrent Flow of Dispersed and Continuous Phase. II: Simulation of Holdup and Particle Size Distribution Profiles," *Chem. Eng. Sci.*, **34**, p. 1151 (1979b).

Korchinsky, W. J., and J. J. C. Cruz-Pinto, "Mass Transfer Coefficients—Calculation for Rigid and Oscillating Drops in Extraction Column," *Chem. Eng. Sci.*, **34**, p. 551 (1979).

Miyauchi, T., and T. Vermeulen, "Longitudinal Dispersion in Two-Phase Continuous Flow Operations," *I.E.C. Fund.*, **2**, p. 113 (1963).

Olney, R. B., "Droplet Characteristics in a Countercurrent Contactor," *AIChE J.*, **10**, p. 827 (1964).

Pratt, H. R. C., and W. J. Anderson, "On Axial Mixing and the Design of Packed Extraction Columns from First Principles," *Proc. Int. Solv. Extn. Conf.*, Can. Inst. Met. Special, **21**, p. 242 (1979).

Pratt, H. R. C., and M. O. Garg, "Scale-up of Backmixed Liquid Extraction Columns," *I.E.C. Process Des. Dev.*, **20**, p. 489 (1981).

Rod, V., "Calculation of Extraction Columns with Longitudinal Mixing," *Brit. Chem. Eng.*, **9**, p. 300 (1964).

Rod, V., "Calculating Mass Transfer with Longitudinal Mixing," *Brit. Chem. Eng.*, **11**, p. 483 (1966).

Rozen, A. M., and A. I. Bezzubova, "Mass Transfer in Individual Drops," *Foundations Chem. Eng.*, Consultant's Bureau Trans. **2**, p. 715 (1968).

Sleicher, C. A., "Axial Mixing and Extraction Efficiency," *AIChE J.*, **5**, p. 145 (1959).

Sleicher, C. A., "Entrainment and Extraction Efficiency of Mixer-Settlers," *AIChE J.*, **6**, p. 529 (1960).

Sovova, H., and J. Prochazka, "Breakage and Coalescence of Drops in a Batched Stirred Vessel. I: Comparison of Continuous and Discrete

Models," *Chem. Eng. Sci.*, **36**, p. 163 (1981).
Sovova, H., "Breakage and Coalescence of Drops in a Batch Stirred Vessel. II: Comparisons of Model and Experiments," *Chem. Eng. Sci.*, **36**, p. 1567 (1981).
Valentas, K. J., and N. R. Amundsen, "Breakage and Coalescence in Dispersed Phase Systems," *I.E.C. Fund.*, **5**, p. 533 (1966).
Vermijs, H. J. A., and H. Kramers, "Liquid-Liquid Extraction in a 'Rotating Disc Contactor'," *Chem. Eng. Sci.*, 3, p. 55 (1954).
Weber, M. E., "Mass Transfer from Spherical Drops at High Reynolds Numbers," *I.E.C. Fund.*, **14**, p. 365 (1975).

Supplementary material has been deposited as Document No. 04176 with the National Auxiliary Publications Service (NAPS), c/o Microfiche Publications, 214-13 Jamaica Avenue, Queens Village, N.Y. 11428, and may be obtained for $4.00 for microfiche or $7.75 for photocopies.

Manuscript received January 4, 1982; revision received April 12, and accepted May 10, 1983.

Complex Nature of the Sulfation Reaction of Limestones and Dolomites

E. Y. CHANG and GEORGE THODOS

Northwestern University
Evanston, IL 60201

Experimental information available in the literature for the sulfation of a wide variety of calcined limestones and dolomites has been used to establish rates of reaction over their entire range of conversion. The reaction rate was found to decay exponentially with extent of conversion and implicated parameters related to two factors, each factor representing a diffusional resistance. These factors define two generalized constants which permit the prediction of the decaying parameters associated with the sorptive capacity of the sorbent.

The sorptive capacity, x_∞, which represents the ultimate conversion of the solid sorbent, has been found to depend on the pore size distribution, the chemical composition of the limestone and/or dolomite and its accessible pore surface area. The combined contribution of x_∞ along with predicted parameters permit the calculation of conversion vs. time relationships that are found in close agreement with experimental measurements for the ten sorbents investigated, with the exception of one.

SCOPE

The sorptive capacity of limestone and/or dolomite for the removal of sulfur dioxide, generated within a fluidized-bed coal combustion facility, is limited because these sorbents do not react to completion in order to satisfy their stoichiometric requirement. This anomaly arises from the volume increase associated as CaO reacts to $CaSO_4$, thus making the interior of a particle only partially accessible to the reaction.

Several models have been advanced in the literature to account for the diffusional effects which relate the rate of sulfation with time. Of note are the grain models of Pigford and Sliger (1973) and Hartman and Coughlin (1976) and the pore model of Chrostowski and Georgakis (1978). These analytical models involve complex numerical integrations in order to predict the rate-decreasing behavior of the sorption reaction. In this context, Lee and Georgakis (1981) point out the computational difficulties encountered with these models that make prohibitive their application to fluidized-bed coal combustion.

The sorptive capacity has been found to vary significantly among solid sorbents. The porosity of the calcined sorbent has been found to exert a major influence on the sorptive capacity; however, no acceptable method is yet available for predicting this capacity without taking a recourse to experimental verification.

CONCLUSIONS AND SIGNIFICANCE

Experimental data for the sulfation of ten calcined limestones and dolomites, obtained at the Argonne National Laboratory, have been critically analyzed to establish the reaction rate parameters and the extent of conversion of each sorbent. From this analysis, it is proposed that the reaction rate can be represented by the exponentially combinational decaying form as,

$$r = r_0 e^{-ax} \cdot e^{-bx^n}$$

where a and b are decaying parameters found to relate directly to two generalized constants α and γ, respectively and the exponent n which relates to the $CaCO_3$ content of the solid sorbent. For their definition, constants α and γ are associated with factors η and φ which represent the pore diffusional resistance and the solid product layer diffusional resistance, respectively.

The extent of conversion from calcium oxide to sulfate, x_∞, has been found to relate to the total intergranular surface area, the calcium to magnesium ratio and the pore size distribution of the solid sorbent after calcination. This behavior has been presented graphically, and together with predicted values of a, b, n and r_0, enabled the establishment of conversion versus time relationships which are in close agreement with the original experimental measurements with all sorbents, with the exception of one, Limestone 1336. An explanation is advanced for the disparity in correlation associated with this stone.